



Michigan Technological University
Create the Future Digital Commons @ Michigan Tech

Dissertations, Master's Theses and Master's
Reports - Open

Dissertations, Master's Theses and Master's
Reports

2009

AFRC Translation Experiments for Space Propulsion

Carrie S. Niemela
Michigan Technological University

Follow this and additional works at: <https://digitalcommons.mtu.edu/etds>



Part of the [Mechanical Engineering Commons](#)

Copyright 2009 Carrie S. Niemela

Recommended Citation

Niemela, Carrie S., "AFRC Translation Experiments for Space Propulsion", Master's report, Michigan Technological University, 2009.

<https://doi.org/10.37099/mtu.dc.etds/716>

Follow this and additional works at: <https://digitalcommons.mtu.edu/etds>



Part of the [Mechanical Engineering Commons](#)

Proposal for Ph.D. Research

AFRC Translation Experiments for Space Propulsion

Carrie S. Niemela
Mechanical Engineering
Michigan Technological University

Annular field reversed configurations (AFRC) plasma devices produce plasma toroids, which can be ejected (translated) at high velocity. This research proposes to investigate AFRC devices for space propulsion by measuring the translation properties of its plasmoid, including velocity, momentum, and efficiency. These measurements demonstrate how well AFRCs can operate as high power electric propulsion technology. The AFRC translation experiment will be constructed in MTU's Ion Space Propulsion Lab, with the design aid of an annular electromagnetic launcher model and magnetic field modeling. The annular electromagnetic launcher model simplifies the motion of the plasmoid using circuit analysis to provide scaling laws for experimental design. These scaling laws, paired with magnetic field modeling, will identify a set of operating conditions and geometry for which translation of the plasmoid is possible. Experimental studies using these operating conditions and a variety of plasma probes will be used to collect data from a translating plasmoid. A time-of-flight array using triple probes and magnetic field probes will capture the average velocity, while a ballistic pendulum will measure its momentum. Efficiency of the process can then be estimated by comparing the final kinetic energy of the plasmoid to the energy initially stored in the capacitor. Finally, scaling laws adapted from the launcher model will be used as a means for comparing AFRC devices to similar pulsed inductive plasma accelerators.

Intellectual Merits: The research proposed here starts by developing AFRC scaling laws from a numerical translation model to provide a solid foundation for designing the experimental apparatus. The experiment itself will provide documented proof of the translation properties of AFRC plasmoids, potentially providing a new technology for high power electric propulsion. The scaling laws are a new tool for AFRC research and give a metric for comparing AFRCs to similar devices, advancing knowledge and understanding of pulsed inductive plasma devices in the space propulsion community. As successful AFRC translation has never been published, understanding the translation dynamics will also benefit the fusion research community, where AFRC technology originated in the quest for low-voltage fusion. The ISP Lab at Michigan Tech is dedicated to the study of electric propulsion in refining traditional technologies and developing advanced concepts. The ISP Lab has numerous vacuum facilities, plasma diagnostic capabilities, and a new FRC facility to accommodate AFRC research. Miss Niemela is a 3rd year graduate student with a BSME from MTU and over 2 years of experience in AFRC research. Her graduate career at MTU has been supplemented by 3 extensive internships at AFRL on Edwards AFB. At AFRL, Miss Niemela facilitated in the design, construction, and testing of the first AFRC translation experiment. Prior to AFRC research at AFRL, she conducted numerical studies on plasma plumes. The studies presented in this proposal build on her previous research experience, focusing the direction of AFRC research and refining the current technology.

Broader Impacts: This research advances discovery and understanding bringing innovative research into the academic setting. This provides teaching opportunities for the researchers during impromptu lab tours and research forums. The multi-disciplinary aspects of this research encourage the participation of several academic departments, including electrical engineering, physics, and mechanical engineering. More importantly, in the university setting undergraduate researchers will have a chance to participate in cutting-edge research, fostering and inspiring scientific discovery. As an example, Adam Heskitt, an Honors student and freshman at MTU, recently participated in a side-project for this research designing and constructing magnetic field probes. This experience helped him use the concepts he learned in classroom for real-life applications. Since this research requires the development of pulsed plasma diagnostics and high power technology, the addition of these to MTU's ISP Lab will make it a premier center for pulsed plasma research. Comparing this device against similar devices improves collaboration among the propulsion community by promoting discussions, sharing technological advances, and merging ideas. Select findings of this research will be published in technical journals, presented at plasma and space propulsion conferences, and shared with other members of the scientific community during lab visits. The benefits this research has on society push beyond technological solutions to promote education, cooperation, and scientific discovery.

PROJECT DESCRIPTION

1 Motivation for Research

Pulsed inductive plasma accelerators produce robust, high power-density plasmoids which can be accelerated to high velocities. Inherent to their pulsed nature, they can be throttled for variable thrust and specific impulse with little change in efficiency. Formation through inductive methods minimizes electrode erosion, ensuring longevity. These characteristics make them attractive for high power electric propulsion. Annular field-reversed configurations (AFRC) are pulsed inductive plasma accelerators which form plasmoids with low energy consumption (250 J/pulse), suitable for spacecraft use. In comparison, other inductive devices require energies exceeding 4 kJ per pulse. Numerous formation studies have been conducted on AFRCs (1) (2) (3) (4) yet no successful studies of plasmoid translation have been published. Before AFRCs can be realized as a high power electric propulsion technology, their plasmoid translation must be characterized. This research seeks to explore AFRCs for high power electric propulsion by demonstrating the translation of these plasmoids, beginning from numerical models.

2 Background: AFRC Overview

An annular field reversed configuration is a compact plasma toroid formed in the annular region between two coaxial coils, as shown in Figure 1. It is a low-voltage derivative of the traditional FRC which is formed without the inner coil. The coils induce a toroidal (azimuthal) diamagnetic current in the plasma, setting up a closed poloidal \mathbf{B} -field. Like other compact toroids, this closed \mathbf{B} -field confines the plasma and allows it to be ejected as a whole from its formation chamber. The plasma toroid retains its shape until dissipative processes disrupt and terminate the confinement. Naturally, it is critical to eject the AFRC while it is still coherent. Its lifetime τ_L is typically 20-30 μs (5).

The formation method for AFRCs varies depending on the coil configuration. The inner and outer coils can be operated in either parallel (synchronous) or independent (asynchronous) mode. In parallel mode, the coils are attached to the same capacitor bank so that the voltages on each coil rise and fall together. In the independent mode, the coils are attached to separate capacitor banks and can be discharged independently from each other. From a spacecraft standpoint, it is desirable to operate the coils in parallel as this requires the least amount of hardware. A brief description of the formation modes is provided in following sections. Each method uses a pre-ionization stage, during which the propellant is partially ionized using any variety of techniques. This allows the propellant to respond to the currents in the coils. Though pre-ionization is a critical part of the discharge (6), it has been investigated for AFRCs elsewhere (4) and will not be the subject this work. Also, it should be clarified that formation of AFRCs remains an empirical process that is not well-understood. The plasma is turbulent fluid, subject to complex magnetohydrodynamic instabilities requiring numerical plasma studies to resolve. End effects, which complicate this discussion but are very important to the confinement, only receive cursory treatment here.

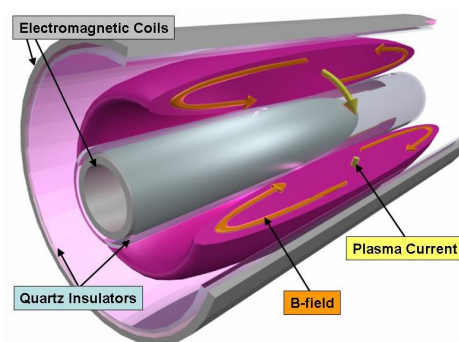


Figure 1: Annular Field Reversed Configuration Schematic. The poloidal \mathbf{B} -field is supported by a toroidal (azimuthal) plasma current.

2.1 Parallel mode

Figure 2A displays the circuit configuration, typical current waveforms, and the formation sequence for the parallel coil operation. The channel between the coils is filled with an inert gas (Step 1), which is then pre-ionized (Step 2). Upon completion of the pre-ionization stage, the capacitors are discharged into the

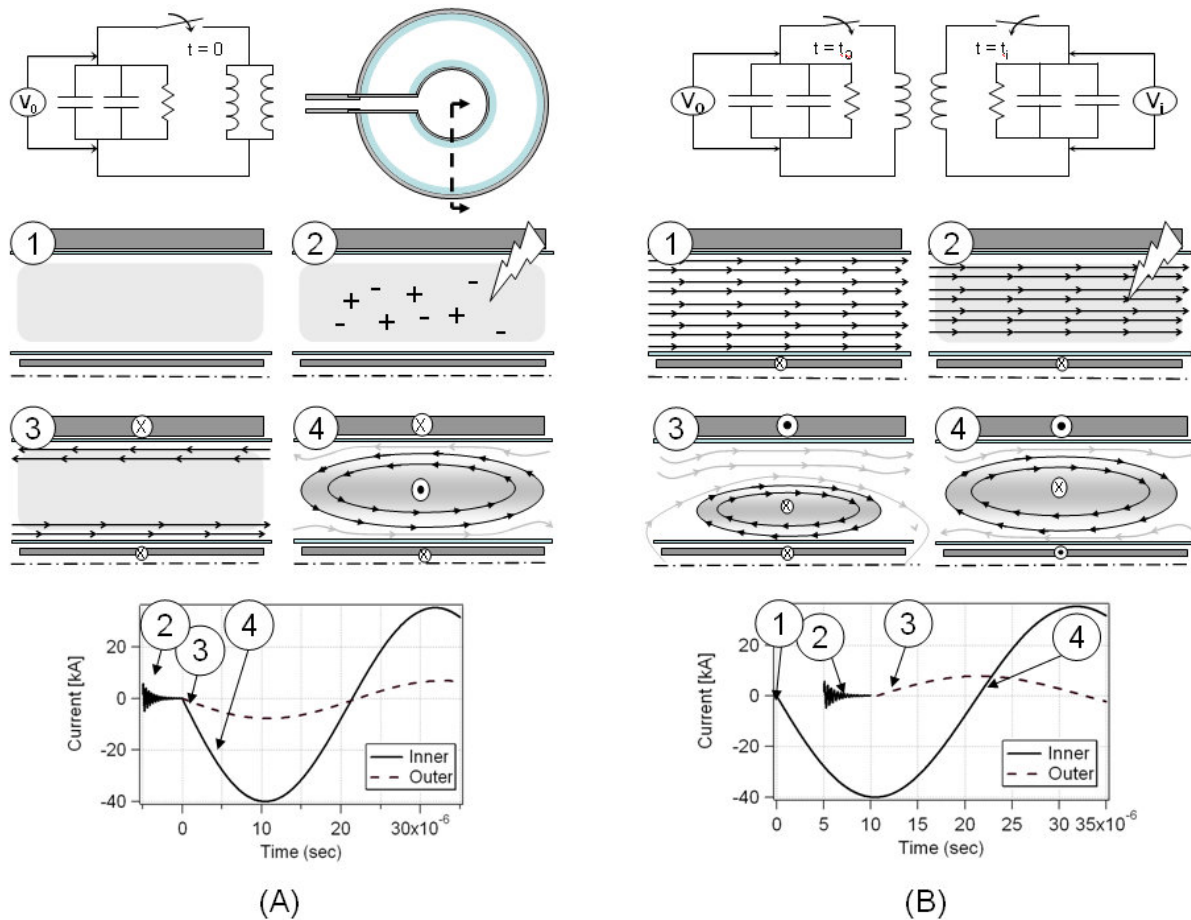


Figure 2: Circuit diagrams, schematics, and waveforms for coil operation mode in the parallel configuration (A) and the independent configuration (B).

coils adding oppositely directed magnetic fields in the annulus between the coils (Step 3). As a consequence of Faraday's Law, the rising currents in the coils cause a current to develop in the plasma, opposing this change in field (Step 4). This current is diamagnetic so that it creates a closed \mathbf{B} -field topology to confine the plasma. Further increasing the currents in the coils causes the current in the plasma to increase, ionizing and heating it. External magnetic pressure from both coils balances with the plasma pressure to help keep the toroid well-centered in the annulus. Confinement of the plasma is improved if oppositely directed field lines near the coil ends are allowed to tear and reconnect, though evidence of this remains unclear.

2.2 Independent mode

Figure 2B shows the circuit configuration, typical current waveforms, and the formation sequence for independent coil operation. Before the start of the discharge, the area between the coils is filled with gas. At $t=0$, the inner coil circuit is discharged. This fills the annulus with a uni-directional \mathbf{B} -field (Step 1). Once this field reaches its maximum strength, the gas is pre-ionized to "freeze" the field into the plasma (Step 2). The outer coil circuit is then discharged in the opposite direction as the current in the inner coil, increasing the total magnetic field inside the annulus. The conducting plasma tries to oppose this increase in field by developing a plasma current that is in the same direction as that of the inner coil. As a result, the plasma becomes strongly attracted to the inner coil. The direction of the plasma current results in a magnetic field that reverses the field direction near the inner coil and sets up the closed \mathbf{B} -field structure in the plasma. The field lines from the inner coil wrap around the outside of the plasma, such that the plasma separatrix

(boundary) is attached to the inner coil (Step 3). When the inner coil current passes through zero and the direction of the magnetic field from the inner coil changes, the plasma is forced off the wall by the current repulsion (Step 4). Magnetic flux is added to both sides of the configuration, resulting in a magnetic pressure that radially balances the plasma. As in the parallel configuration, increasing the coil current, induces a stronger plasma current to further ionize and heat it.

2.3 Translation of AFRCs

Though translation studies on AFRCs have never been published, it could be done in the same manner as traditional FRCs. In these devices, expulsion of the plasmoid from the discharge chamber is done using a variety of methods, including a conical discharge coil (7), gated "kicker" coils (8), impurity injections (9), and magnetic plungers. A conical discharge coil requires the least amount of hardware and this method will be used in this research. The conical coil, as shown in Figure 3, forms a small component of radial magnetic field to interact with azimuthal plasma current to create an axially directed Lorentz force $\mathbf{J} \times \mathbf{B}$ on the plasmoid. It is critical that this Lorentz force is large enough to expel the plasmoid on a timescale less than the plasmoid lifetime τ_L (20-30 μs (5)).

Translation of an AFRC can occur only if the configuration is magnetically detached from the coils. Magnetic detachment should occur naturally in the parallel coil configuration since the plasmoid is formed in the null-field region of the coils and ideally, no field lines tie it to the coils. In the independent operation, the configuration becomes detached from the coils only after it lifts off the inner coil.

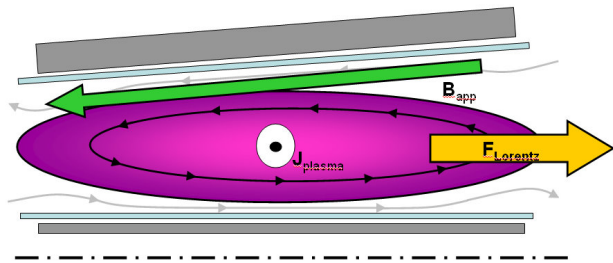


Figure 3: Conical discharge coil used to translate the plasmoid. The radial component of \mathbf{B} interacts with the azimuthal \mathbf{J} for an axially directed F_{Lorentz} .

3 Literature Review

3.1 Previous AFRC and FRC Research

Annular FRCs were first proposed by Phillips (2) in 1981 as a means of producing large compact toroids for fusion research. His device "Slingshot" demonstrated that it was possible to form a plasma ring between two coaxial coils. The Slingshot and similar experiments on annular FRCs (10) (11) were conducted using moderate coil voltages (20 kV) to drive current through the coil on fast time scales (5 μs). Since the voltage across the coil (an inductor) is proportional to dI/dt , it is possible to decrease this voltage and drive the same amount of current by operating on a slower timescale. This eliminates the need for ultra-high voltage capacitors and fast switching. Low formation voltage experiments were demonstrated with the Coaxial Slow Source (1) (2) (3) at the University of Washington. This experiment showed that it was possible to form annular FRCs at low voltages (1 kV) and on slow timescales (100 μs). This way, energy is transferred to the plasma through resistive-diffusive heating rather than through shock heating. Work on the CSS was discontinued when it was found that the plasma temperature (20 eV) and densities (10^{21} m^{-3}) were insufficient for fusion. Inspired by the low-voltage formation technologies required for spacecraft integration, the Air Force Research Laboratory (AFRL) recently demonstrated slow formation of AFRCs at spacecraft-adaptable voltages of 500 V - 1 kV and energy levels of 250 - 450 J per pulse (4).

Though AFRCs are intended to be translated into a true FRC with no structure penetrating the core of the plasma, translation studies on AFRCs were not presented until recently (12). This experiment, the XOCOT-T, built on the AFRC formation study by Kirtley at AFRL (4). An AFRC translation experiment was constructed and operated with two different conical outer coils. The first attempt was made with a small 1.6° cone and later a 5° cone was used. Discharge voltages up to 2 kV were tested. Though magnetic field

activity inside the discharge coils signaled the formation of an AFRC, translation of the plasmoid was not evident.

Translation dynamics for traditional FRCs (6) have been well-studied (7) (8) (13) (14). Studies have shown that these plasmoids do not change their magnetic field topology significantly during translation. These devices use very high voltages (200 kV) over short timescales (5 μ s) and translation occurs in a flux-conserving region. As such, FRCs have a much higher energy content and different plasma dynamics than the low-voltage AFRC plasmoid, making their application to space propulsion limited.

An alternate concept to low-voltage FRC formation is through the use of rotating magnetic fields (RMF) to drive an azimuthal electron current (15). An experiment that mates an RMF FRC source to a stage of acceleration coils for the purpose of space propulsion is currently being investigated by MSNW (16). Power levels of several MW are expected, well beyond the capabilities of current spacecraft technology.

3.2 Previous Pulsed Inductive Plasma Research

Annular FRCs belong to the class of pulsed inductive plasma accelerators. These are devices which use flat plates, theta pinch coils, or conical theta pinch coils to form and accelerate a plasmoid or current sheet. A brief description of this group is given in the text by Jahn (17). For spacecraft applications, the only system that has been fully characterized is the Pulsed Inductive Thruster (PIT) (18). The PIT uses a 1-m diameter flat plate (which can be thought of as a 90° cone) to induce a large azimuthal current in a layer of gas. Current repulsion (same as the Lorentz force) of the azimuthal induction current and the azimuthal driving current propels the plasma downstream with a high specific impulse (up to 8,000 s). Since the plasma is accelerated from the plate as soon as plasma currents develop, poor coupling exists between the coil and plasma. Additionally, the gas must be ionized and accelerated in a very short amount of time, requiring coil voltages of 32 kV and 4 kJ of energy per pulse. The Faraday Accelerator with Radio-Frequency Assisted Discharge (FARAD) proposes to lower the energy per pulse to 44 J by adding an rf pre-ionization stage with the flat-plate accelerator(19) or a conical theta-pinch coil (20) to drop the pulse energy to 44 J/pulse (with 1 kW of pre-ionization). Testing on this device is still preliminary.

Another technology for creating and accelerating plasmoids is a spheromak-based thruster. Though a full characterization of this device is unavailable, it has received some attention during the Plasmoid Thruster (PTX) Experiment (21). This experiment formed the plasmoid inside a short, 17.5° conical theta pinch coil. Though forming the plasmoid inside a conical coil results in better coupling between the plasmoid and coil (the two are allowed to interact over a longer distance), formation voltages of 35 kV are still required. A new generation of the PTX, the PT-1, strives to drop the discharge voltage to around 6 kV and 280 J/pulse (22) through circuit optimization, but performance numbers are not available.

4 Proposed Research Overview

To demonstrate AFRCs as a high power electric propulsion technology, this research proposes to measure the translation properties of an AFRC plasmoid, including its velocity, momentum, and efficiency. A new AFRC translation experiment for taking these measurements will be constructed in MTU's Ion Space Propulsion Lab. This experiment will be designed with the aid of an annular electromagnetic launcher model and magnetic field modeling to identify a set of operating conditions, such as cone angle, voltage, plasmoid mass, etc., for which translation of the plasmoid is possible. Experimental studies using these operating conditions and a variety of plasma probes will be used to collect data from a translating plasmoid. A time-of-flight array using triple probes and magnetic field probes will capture the average velocity, while a ballistic pendulum will measure its momentum. Efficiency of the process can then be estimated by comparing the kinetic energy of the plasmoid to the energy initially stored in the capacitor. Finally, AFRC devices will be compared to similar pulsed inductive plasma accelerators using the scaling laws derived from the launcher model.

The main objective of this research is to measure the translation characteristics of an AFRC plasmoid. This includes taking plasmoid velocity and momentum measurements, as well as estimating the efficiency of the formation and translation processes. Efficiency is defined as ratio of final kinetic energy to initial energy stored in the capacitor bank. A secondary objective of this research is to compare the translation

properties of AFRC devices to other pulsed inductive thrusters, such as the PIT and the PTX, using numerical methods. Additionally, the experimental measurements can be compared to results from the analytic-numerical model to demonstrate how effectively such mathematical tools can be used in the future design of AFRC translation experiments. The remainder of this report will focus on the methodology and research plan proposed to satisfy these objectives.

5 Methodology

The research proposed here will use an analytic-numerical model, an electromagnetic field solver, and experimental hardware to investigate the research objectives outlined in Section 4.

5.1 Methodology for Experimental Design

The AFRC translation experiment will be designed by considering both the energy requirements necessary for translation and the magnetic field topogology. First, a coil geometry and circuit design must be found that allows the Lorentz force to expel the plasmoid from the channel in a sufficiently short amount of time ($\tau_{ACC} \leq \tau_L$). Then, it must be shown that this geometry does not tie the plasmoid to the coils and that it provides radial stability to keep the plasma well-centered in the formation chamber. An analytic-numerical model (described in Section 6.1), using a mathematical description of an annular electromagnetic launcher will be used to develop scaling laws for AFRC plasmoid accelerators. These scaling laws can isolate the critical design parameters, providing an efficient means for determining a set of conditions that satisfy $\tau_{ACC} \leq \tau_L$. The following list of conditions will be considered: coil angle, discharge voltage, coil inductance (turns, radius, length), line inductance, capacitance, and propellant type. The plasma conditions are difficult to specify without an experiment so a range of plasma temperatures, densities, and volumes will be used. Magnetic field modeling of the final geometry will be mapped using commercial electromagnetic field solvers, such as those available in COMSOL.

5.2 Methodology for AFRC Translation Study

Once operating conditions for the experiment have been found, experimental hardware for forming and translating AFRCs will be constructed with circuit parameters and coil designs that satisfy these conditions. The apparatus will be designed with both a stationary discharge coil and a translation coil. The stationary coil will allow measurements of the plasma properties (temperature, density, excluded magnetic flux) for benchmarking purposes. Following the stationary coil studies, the outer coil will be exchanged for a conical discharge coil to study plasma translation. A time-of-flight array using triple probes and magnetic field probes will be constructed to measure the plasmoid velocity. A ballistic pendulum will also be designed and constructed to measure the plasmoid's momentum. Design specifics of both diagnostics are discussed in Section 6.3. The efficiency of the AFRC device will be calculated from these diagnostics by comparing the final velocity and entrained mass to the initial energy stored in the capacitor. Downstream measurements of plasmoid velocity, momentum, and efficiency will provide basic performance statistics to determine how well AFRCs lend themselves to high power electric propulsion technology.

5.3 Methodology for Device Comparison Study

Using the annular electromagnetic launcher model that has been developed for this research, it is possible to compare the AFRCs with similar technologies such as the spheromak plasmoid thruster (PTX) and the pulsed inductive thruster (PIT). The PTX and PIT have been previously analyzed using numerical techniques (23) (24). The annular model can be adapted to resemble these geometries with inclusion/exclusion of a few variables. The governing equations can then be reformatted (non-dimensionalized) to provide a side-by-side comparison of the technologies.

6 Technical Statement of Work

The numerical and experimental tools to be used in this research are described in the following section.

6.1 Annular Electromagnetic Launcher Model

Dynamic models are a popular technique for analyzing pulsed plasma technologies (17), pulsed inductive plasmoid accelerators (18) (23) (24), and electromagnetic launchers (25). These models allow a complex system to be simplified into a collection of circuit elements which can be solved with a set of first order ordinary differential equations, rather than computationally intense particle codes.

In the manner of other dynamic models, the model developed for this research treats the plasmoid as a rigid conducting slug, translated from its formation chamber under an axially directed Lorentz force. The plasmoid is magnetically coupled to the coils through mutual inductance, which decays as it travels downstream. The mutual inductance dictates the interaction of the plasma current and the coil current which control the Lorentz force. The currents can be found using circuit analysis. This study adds to the complexity of the previous translating slug models with the addition of the center coil; no previous studies have been presented with an inductive coaxial-slug launcher. In addition to modeling the physics of the electromagnetic acceleration, the model also attempts to capture the gas-kinetic acceleration of the plasmoid by allowing for internal-kinetic energy exchange due to the plasma's high temperature and gas dynamic properties. This is done by assuming a temperature profile $T(z)$ which changes with the plasmoid's position. Figure 4 provides a pictorial overview of the annular electromagnetic launcher model, operating in the parallel coil mode.

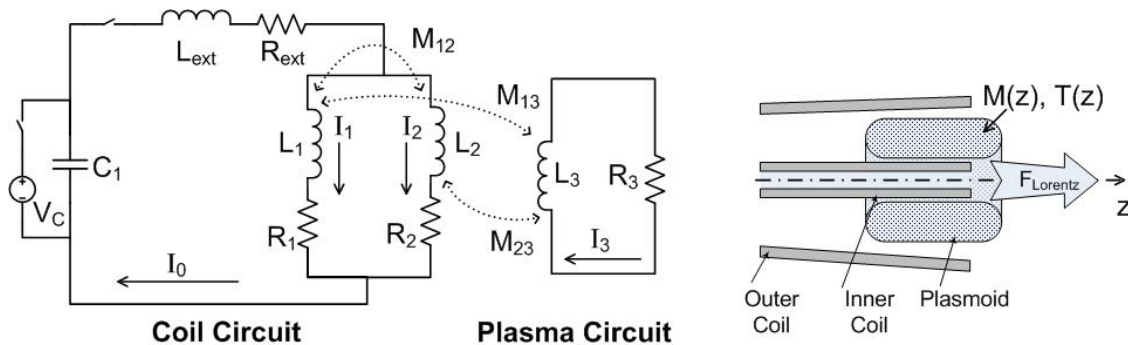


Figure 4: Schematic of annular electromagnetic launcher model. Coils operating in parallel.

A complete mathematical description of the model consists of 7 coupled non-linear ordinary differential equations: 5 circuit equations and 2 equations of motion. The system of equations is introduced in following sections. These equations can be solved using any variety of numerical integration methods. The solver chosen for this work is the ode45 solver, available in MathWork's MatLab. It is an explicit 4th order Runge-Kutta solver, ideal for medium-accuracy, non-stiff problems.

6.1.1 Equations of Motion

Plasmoid acceleration arising from the Lorentz force can be found by directly solving the cross product of $\mathbf{J} \times \mathbf{B}$. However, this method becomes tedious, as the functional form of \mathbf{B} contains several elliptic integrals. A more eloquent derivation uses the work-kinetic energy theorem. This theorem states that the work done on an object by conservative forces results in a change in potential energy along the path of motion ($\delta W_c = -\Delta U = \mathbf{F} \cdot \delta \mathbf{z}$). Therefore, the forces acting on the plasmoid in the axial direction F_z can be found by taking the partial derivative of the total potential energy U_{tot} with respect to axial position z . The potential energy U_{tot} of the entire system is a sum of the energy in the magnetic field U_{mag} , the energy in the capacitor bank U_{cap} , and the internal energy stored in the plasma, U_{int} . Only U_{mag} and U_{int} change with plasmoid position. Using this information and Newton's Second Law, the equation of motion for the plasmoid becomes:

$$m \frac{dv_z}{dt} = -\frac{dM_{13}}{dz} I_1 I_3 - \frac{dM_{23}}{dz} I_2 I_3 - \frac{3}{2} N_i k_B \frac{dT}{dz} \quad (1)$$

where

$$v_z = \frac{dz}{dt} \quad (2)$$

In Equation 1, M_{13} is the mutual inductance between the outer coil and plasmoid, M_{23} is the mutual inductance between the inner coil and plasmoid, I_1 , I_2 , I_3 are the outer coil, inner coil, and plasmoid circuit currents, N_i is the ion number density, k_B is the Boltzmann constant, and T is the bulk plasma temperature. Equations 1 and 2 can be solved if the coil currents, plasma currents, mutual inductance profiles, and plasma temperature profile are known. Each of these items will be discussed in the following sections.

6.1.2 Circuit Equations

The coil and plasma currents can be found by considering the system to be a RLC circuit, resembling that shown in Figure 4. The circuits communicate through respective mutual inductances. Applying Kirchoff's Voltage Laws to the circuit shown in Figure 4, the following equations are found:

$$V_C = L_{ext} \frac{dI_0}{dt} + R_{ext} I_0 + L_1 \frac{dI_1}{dt} + M_{12} \frac{dI_2}{dt} + R_1 I_1 - I_3 \frac{dM_{13}}{dt} - M_{13} \frac{dI_3}{dt} \quad (3)$$

where

$$I_0 = I_1 + I_2 \quad (4)$$

$$0 = L_1 \frac{dI_1}{dt} + R_1 I_1 + M_{12} \frac{dI_2}{dt} - M_{13} \frac{dI_3}{dt} - I_3 \frac{dM_{13}}{dt} - L_2 \frac{dI_2}{dt} - R_2 I_2 - M_{12} \frac{dI_1}{dt} + M_{23} \frac{dI_3}{dt} + I_3 \frac{dM_{23}}{dt} \quad (5)$$

$$0 = R_3 I_3 + L_3 \frac{dI_3}{dt} - M_{13} \frac{dI_1}{dt} - I_1 \frac{dM_{13}}{dt} - I_2 \frac{dM_{23}}{dt} - M_{23} \frac{dI_2}{dt} \quad (6)$$

The current induced in the plasma I_3 removes energy from the inner and outer coil circuit; it represents an energy sink where the contributions of M_{13} and M_{23} are negative. The current through the capacitor can be found from:

$$\frac{dV_C}{dt} = -\frac{I_0}{C} \quad (7)$$

Equations 1- 7 represent the complete system of equations describing motion of the plasmoid.

6.1.3 Plasma Resistance

The resistance of the plasma R_3 can be calculated by assuming a fully ionized plasma with uniform properties (density, temperature). Resistivity then arises as a result of Coloumb collisions of the current carrying electrons with stationary ions. Spitzer (26) reports this resistivity for a diamagnetic plasma (like that in an AFRC) in terms of the ion charge number Z , the electron temperature (in eV) T_e , and the Coloumb logarithm $\ln \Lambda$:

$$\rho_{Spitzer} = 1.03 \times 10^{-4} \frac{Z \ln \Lambda}{T_e^{3/2}} \quad (8)$$

The Coloumb parameter Λ is related to the length scale for Coloumb interactions. It is typically a very large number whose logarithm is insensitive to changes in plasma parameters. For an AFRC, $\ln \Lambda$ of 12-15 can be used. Using the estimated resistivity, plasma resistance can be calculated from $R = \rho l / A$, where l is the plasmoid length and A is the cross sectional area.

6.1.4 Inductance Calculations

The self inductance for the outer and inner coils L_1 and L_2 can be approximated using formula handbooks, such as Grover (27) and Lundin (28). The mutual inductance of the inner and outer coils can also be calculated from these formularies.

The inductances of more complicated current distributions, such as the self-inductance of an annular plasmoid L_3 and mutual inductance between the coils and plasmoid M_{13} and M_{23} , can be found using a commercial electromagnetic field solver. Once the fields and current distributions have been solved for, inductance can be found either from magnetic field energy: $L = 2U_{mag}/I_{tot}^2$ or from complex impedance $L = \text{imag}(V_0/I_{tot}\omega)$. The self-inductance is calculated by applying an electric potential V_0 to the desired conductor and leaving the remaining conductors invisible (zero conductivity, permittivity). The mutual inductance between two conductors can be found by applying V_0 to only one of the conductors and setting the other to an appropriate conductivity and permittivity. The current through the constrained conductor changes due to the coupling of the inductors so that its effective inductance L_{eff} is a combination of the self-inductance of both conductors L_{self} , L_{other} and the mutual inductance M between the two as shown in Equation 9. This equation can be verified through a quick circuit analysis and is cited in (18) and (23).

$$L_{eff} = L_{self} - \frac{M^2}{L_{other}} \quad (9)$$

To find the mutual inductance profile of a translating plasmoid $M(z)$, L_{eff} can be found for different plasmoid positions and solved for M . A curve fit to the resulting data allows a functional form of $M(z)$ and dM/dz to be determined. Multiple authors (18) (23) (29) have found the mutual inductance profile for electromagnetic launchers to follow an exponential distribution:

$$M(z) = k_0 \sqrt{L_p L_c} \exp\left(-\left(\frac{z}{z_0}\right)^n\right) \quad (10)$$

where k_0 is the nominal coupling coefficient, L_p and L_c are the projectile and coil inductances, z_0 is the length scale of the coupling, and n relates to the half-angle of the coil. The parameter n increases with decreasing cone angle, approaching $n = 1$ for large cone angles greater than 10° .

6.1.5 Temperature Profile

The plasmoid contains a hot plasma, whose gas pressure pushes against the confining geometry of the conical outer coil. Similar to a gas nozzle, the cone imparts an axial pressure gradient to the plasmoid, resulting in a net axial force out the large end of the cone. This pressure gradient can be related to the temperature of the plasma through principles of gas dynamics, allowing the internal energy in the plasmoid $3/2N_i k_B T$ to be exchanged for directed kinetic energy. Since the physics of this conversion are analogous to a gas expansion through a nozzle, it may be possible to derive a plasma temperature profile $T(z)$ and dT/dz which is dependent on cone angle. This idea will be explored in future work.

6.1.6 Plasmoid Mass Calculation

The mass of the plasmoid can be estimated assuming a uniform plasma density distribution, n_e and approximating the plasmoid volume, V_{ol} . Then, the plasmoid mass is simply $m = n_e V_{ol} M_m / N_A$, where M_m is the molar mass of the plasmoid gas and N_A is Avogadro's number.

6.1.7 Performance Calculations

The momentum of the plasmoid can be calculated if the plasmoid mass and velocity are known. Momentum is simply:

$$p = mv_z \quad (11)$$

Performing a force balance on the plasmoid, it is apparent that the plasmoid's directed momentum imparts a thrust T on the coils which can be found from Newton's 2nd Law:

$$T = m \frac{dv_z}{dt} \quad (12)$$

Efficiency of the system can be defined as a ratio of the final kinetic energy to the initial energy stored in the capacitor:

$$\eta = \frac{mv_f^2}{CV^2} \quad (13)$$

6.1.8 Model Validation

The coil circuit equations (Equations 3, 4, 5, 7) were tested using circuit parameters from the XOCOT-T. These are shown in Table 1. Coil, transmission line, and external inductance values were measured with an Agilent 4294A Impedance Analyzer for the small cone version (cone angle of 1.6°) of the experiment. L_1 and L_2 in Table 1 include line inductances. The external resistance R_{ext} was adjusted to match the damping on the experimental data, since this value was not measured. Mutual inductance between the two coils M_{12} was not taken into account as attempts to do so resulted in mis-matched frequencies.¹ The circuit equations (Equations 3, 4, 5, 7) were solved to find I_0 , I_1 , and I_2 . These were compared to measurements from Pearson current monitors on the XOCOT-T experiment. As is shown in Figure 5, exceptional agreement between the experimental data and the circuit solutions was found. The charging voltage on the experiment was 2 kV, but $V_C = 1444$ V was needed in the model to provide good agreement with the data. (The experimental charging voltage on the capacitors was for references purposes only, so for now the discrepancy is of little consequence.)

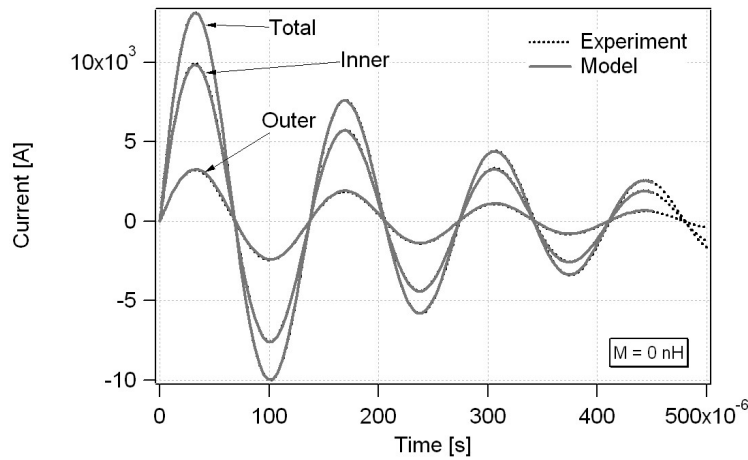


Figure 5: Comparison of circuit currents I_0 , I_1 , I_2 with XOCOT-T experimental data.

Table 1: XOCOT-T Coil Circuit Parameters

V_C	C	L_{ext}	R_{ext}	L_1	R_1	L_2	R_2
1444 V	225 μ F	1.53 μ H	16 m Ω	2.29 μ H	1 m Ω	746 μ H	1 m Ω

¹Mutual inductance is defined as the amount of magnetic flux from one conductor that passes through another's cross sectional area. In the coaxial coil geometry if all the magnetic flux from the inner coil passes through the annulus, the outer coil should see no *net* flux through its cross section from the inner coil. This results in minimal magnetic coupling between the coils, as a consequence of Faraday's Law.

The equations of motion (Equations 1, 2) coupled with the circuit equations (Equations 3, 4, 6, 7) were tested using data published for the ring launcher by Novac (25). The inner coil circuit was ignored by setting $R_2 = 100 \Omega$, L_2 , M_{12} , $M_{23} = 0$. The remaining parameters were set to values from Table 1 in Reference (25): $m = 0.7 \text{ g}$, $C_1 = 31.8 \mu\text{F}$, $L_{ext} = 12.7 \text{ nH}$, $R_{ext} = 1 \text{ m}\Omega$, $L_1 = 63.6 \text{ nH}$, and $L_3 = 74.7 \text{ nH}$. The projectile resistance R_3 was set to $15 \text{ m}\Omega$ and the capacitor charged to 30 kV . The mutual inductance profile was not specified, but Martin and Eskridge who performed a similar validation study on their model used $k_0 = 0.98$, $z_0 = 5 \text{ mm}$, and $n = 1$ with good results. The annular electromagnetic launcher model with these parameters determined the final projectile velocity to be 3.78 km/s , near the 4 km/s terminal velocity reported by Novac. This, combined with the circuit validation outlined in the previous paragraph, shows that the annular electromagnetic launcher model should provide fairly reliable results.

The methodology for finding mutual inductance profiles using electromagnetic software was verified by reconstructing the PTX experiment by Martin and Eskridge (23) in COMSOL's Multiphysics software. The PTX experiment used a conical theta pinch coil of 17.5° with an aluminum slug, machined to fit the coil. They measured an effective inductance profile experimentally and calculated one using QuickField software. Repeating their experiment in COMSOL provided the $L_{eff}(z)$ shown in Figure 6. Comparing this profile to the results obtained by Martin and Eskridge shows good agreement in trend and minimal difference in magnitude. These findings substantiate the computational methods for determining the mutual inductance profile $M(z)$ (as outlined in Section 6.1.4).

6.1.9 Case Study using XOCOT-T Data

A preliminary case study was completed using the data from the XOCOT-T experiment to demonstrate application of the annular electromagnetic launcher model. This study used the circuit parameters verified in Section 6.1.8, with inductances calculated from COMSOL. Both coil versions of the experiment (small and large) were tested. XOCOT-T/v1 had a smaller cone than XOCOT-T/v2 (cone half angle of 1.6° compared to 5°). For this study, only the forces due to the Lorentz acceleration were studied; internal energy effects will be investigated at a later date.

The inductance simulations were set up in COMSOL with a 2D axi-symmetric geometry, time-harmonic solver at a frequency f of 7.233 kHz (the discharge frequency of the experiment), and insulative boundary conditions. The bounding geometry was made sufficiently large to prevent disturbances in the magnetic field around the coils and plasmoid. Skin effects were resolved using boundary layer meshing for the plasma, a fine structured mesh for the inner coil, and an extremely fine tet mesh for the outer coil. The geometry and mesh detail are shown in Figure 7. For this exercise, the tank and backplate were invisible (conductivity of zero) to the fields and currents. Equation 8 was used to find plasma conductivity ($\sigma = 1/\rho$). For a $10 - 20 \text{ eV}$ plasma with a density of $10^{19} \text{ particles/m}^3$, σ_{plasma} is approximately $30,000 - 70,000 \text{ S/m}$. The plasmoid dimensions were chosen to be 28 cm (85 percent of the coil length) by 4.86 cm , centered between the coils. These dimensions are arbitrary, but expected to be the maximum size of an AFRC in the XOCOT-T. Since coupling between conductors degrades with increasing distance from each other, modeling the plasmoid at these dimensions provides the best-case approximation. Sensitivity of the plasmoid acceleration to its geometry will be studied at a later date.

Before calculating the mutual inductance profiles for the system, the self inductances of the inner coil, outer coil, and plasmoid were calculated. This was done by applying a boundary condition of $V_0 = 500 \text{ V}$ to the desired conductor and making all other surrounding objects invisible. The fields and current

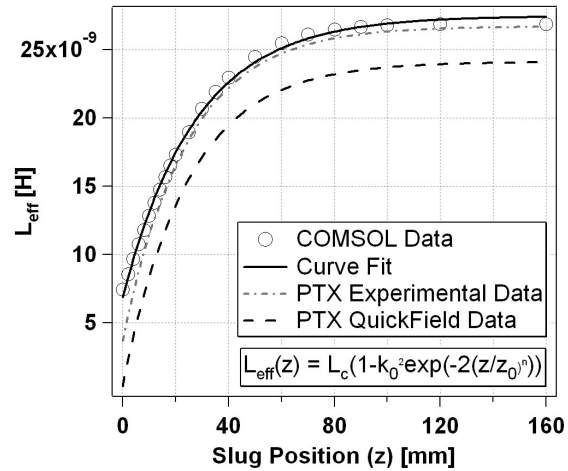


Figure 6: Comparison of effective inductance profiles for the PTX experiment.

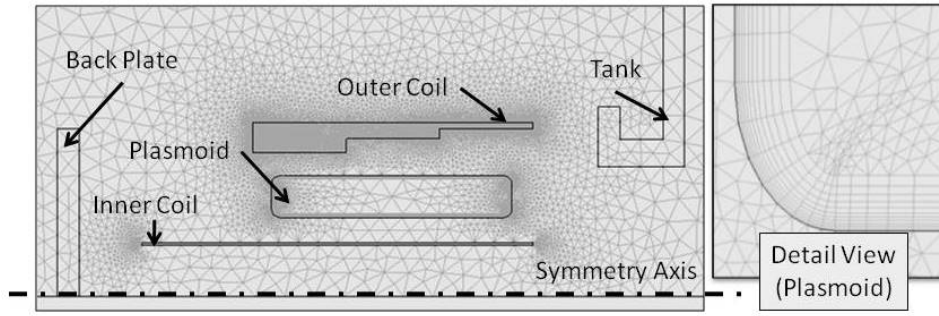


Figure 7: Mesh detail for the XOCOT-T Case Study.

distributions were solved by COMSOL. The self inductance was calculated from the inductive impedance: $L = \text{imag}(V_0/I_{tot}\omega)$, where I_{tot} is the integrated current density (total current) in the plasmod and $\omega = 2\pi f$. The XOCOT-T used multi-turn coils, which cannot be accurately modeled in COMSOL. Since $L \propto N^2$ (see Section 6.1.4), the multi-turn geometry can be modeled as a single-turn coil and the number of turns N accounted for by multiplying the calculated inductance by N^2 . Table 2 displays the results of the COMSOL calculations, comparing this method with the measured inductance and the inductance calculated from Grover (27). The COMSOL method underpredicts the inductance for this geometry, most likely because it does not take into account experimental imperfections (coil connectors, slotted coils, interference, etc). However, it is close enough to the measured and calculated values to provide sufficient confidence in the method.

Table 2: XOCOT-T Coil Inductance Comparison

Object	Calculated Inductance	Measured Inductance at 7.233 kHz	COMSOL Inductance
Outer Coil v1 (3-turns)	2.09 - 2.29 μH	2.29 μH	1.98 μH
Outer Coil v2 (3-turns)	2.09 - 2.70 μH		2.17 μH
Inner Coil v1 (3-turns)	335 nH	348 nH	311 nH
Inner Coil v2 (4-turns)			433 nH
Plasmod			110 nH

The mutual inductance profiles for the inner coil-plasmod and the outer coil-plasmod were calculated separately. First, 500 V was applied to the outer coil, with the inner coil invisible. The effective inductance of the outer coil and the plasmod was found, as outlined in Section 6.1.4. To account for the multi-turns, this effective inductance was multiplied by N^2 of the driving (outer) coil. This is valid since $L_1 \propto N_1^2$, $L_3 \propto N_3^2$, $M_{13} \propto N_1 N_3$. Manipulating Equation 9 shows that the effective inductance of a multi-turn system is N^2 times L_{eff} of a single-turn system. When this procedure was complete, the outer coil was made invisible with the inner coil activated. The effective inductance of the system was again calculated. The plasmod was moved to a new axial location and the procedure repeated. The effective inductance (compensated for by N^2) of both systems was solved for M using equation 9. An exponential curve in the form of Equation 10 was fit to the data. For $\sigma_{plasma} = 30,000 \text{ S/m}$ and the small cone angle, $k_{13} = 0.586$, $z_{13} = 0.320 \text{ m}$, $n_{13} = 2.18$, $k_{23} = 0.461$, $z_{23} = 0.296 \text{ m}$, and $n_{23} = 2.455$. The coefficients are similar for $\sigma_{plasma} = 70,000 \text{ S/m}$ and for the larger cone. Figure 8 displays the resulting profiles for M_{13} and M_{23} . From this graph, it can be deduced that while the small cone has a larger maximum dM/dz , the large cone increase in dM/dz sooner (up until the maximum dM/dz). Since dM/dz is proportional to the Lorentz force, this means the large cone will have a larger Lorentz force than the small cone while the plasmod is still inside the coils, but once the plasmod is partly outside the coils (in the region of maximum dM/dz), the smaller coil will create

a greater Lorentz force for equivalent currents.

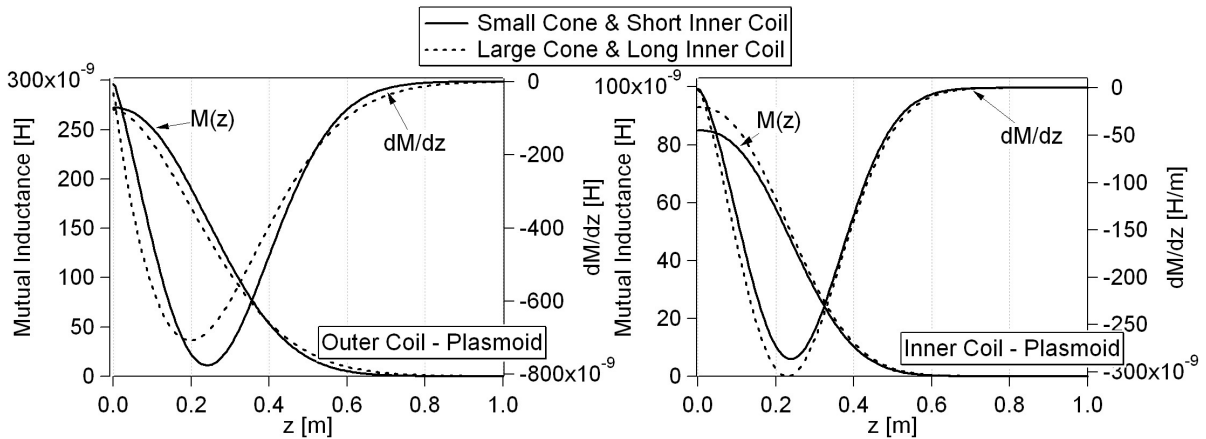


Figure 8: $M(z)$ and dM/dz for the XOCOT-T. Plasma conductivity is 30,000 S/m.

The mutual inductance profiles M_{13} , M_{23} and their derivatives dM_{12}/dz , dM_{23}/dz for both versions of the XOCOT-T were inserted into the annular electromagnetic model (schematically described in Figure 4), along with the circuit parameters from Table 3. The coil inductances L_1 and L_2 include external transmission line inductances. For now, temperature exchange with kinetic energy is ignored. Plasma resistance was calculated to be about 0.1 m Ω , using a Spitzer resistivity of 14 - 33 $\mu\Omega$ m. The mass of the plasmoid, using a density of 3×10^{19} m $^{-3}$ and Argon gas, was 2×10^{-8} kg. The plasmoid was assumed to be instantly formed with no initial current and velocity. It was radially centered between the coils, slightly ahead of the axial midplane of the coils at $z = 1$ mm (to avoid a singularity resulting from the $M(z)$ curve fit). MatLab's ode45 solver was then used with 1, 2, and 3 - 7 to calculate a time history of I_1 , I_2 , I_3 , V_C , v_z , and z . The plasmoid momentum and thrust were calculated using Equations 11 and 12, respectively. Figure 9 shows the results for both versions of the XOCOT-T for two different plasma conductivities (corresponding to 10 eV and 20 eV).

Table 3: XOCOT-T Circuit Parameters

	V_C	C	L_{ext}	R_{ext}	L_1	R_1	L_2	R_2
1	1444 V	225 μ F	1.53 μ H	16 m Ω	2.29 μ H	1 m Ω	746 μ H	1 m Ω
2	1444 V	225 μ F	1.53 μ H	16 m Ω	2.31 μ H	1 m Ω	844 μ H	1 m Ω

The outer coil is 33 cm long; when the plasmoid is at $z = 16.5$ cm, it is halfway out of the coils. From Figure 9, it can be noticed that the small cone is not sufficient to accelerate the plasmoid out of the discharge chamber; for both plasma conductivities, the axial position of the plasmoid never reaches the end of the coil (indicated by the dotted horizontal line). While the large cone does appear to accelerate the plasmoid out of the coil region, the time it takes to do this is greater than the lifetime of an AFRC plasmoid (20 - 30 μ s). A higher plasma conductivity (corresponding to a higher plasma temperature) results in a slightly higher velocity, though it is still insufficient to propel the plasmoid from the coils in time.

If the plasmoid configuration lifetime could be increased to over 50 μ s, the plasmoid in the XOCOT-T could reach a maximum velocity of 40 km/s, imparting a force of 68 N on the coils. Using Equation 13, the total efficiency of the system would be 6.8 percent.

This study demonstrates the application of the annular electromagnetic launcher model. It shows that, for a typical AFRC experiment operating at voltages less than 2 kV, the Lorentz force between the plasmoid and the coils is not large enough to accelerate the plasmoid from the formation chamber in a sufficiently short amount of time ($\tau_{ACC} \leq \tau_L$). By adjusting the input parameters to the model, it may be possible to find a set of conditions that satisfy ($\tau_{ACC} \leq \tau_L$). This exercise can be expedited with non-dimensional analysis and will be left for future investigation.

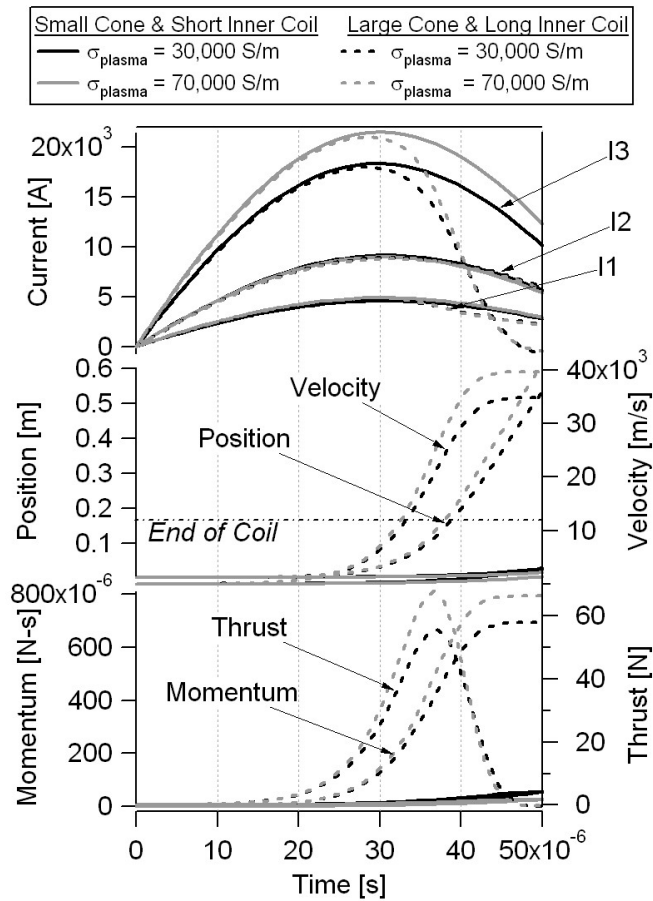


Figure 9: I_1 , I_2 , I_3 , v_z , z , momentum, and thrust predictions for the XOCOT-T at different plasma conductivities. Plasmoid position is tracked with respect to its center.

6.2 Magnetic Field Modeling

The magnetic field topology for forming and stabilizing an AFRC requires that equal magnetic flux is added to the configuration from both coils. In equilibrium, this will keep the configuration radially centered since the magnetic pressure can balance the plasma pressure. The magnetic field for a coaxial coil geometry containing a conductive "plasma" can be modeled using COMSOL's electromagnetic field solvers to ensure an equal flux distribution. If the coils alone do not produce such a flux distribution, it is possible that conducting objects can be strategically placed near the coils to facilitate flux shaping. Though time-harmonic solvers are appropriate for an AFRC discharge, transient solvers are also available to plot a time-history of the entire formation sequence.

6.3 Proposed Apparatus and Diagnostics

The proposed experimental apparatus, the TeXOCOT, is a next-generation device of the XOCOT-T. A skeleton of the design currently resides in Michigan Tech's Ion Space Propulsion Lab, attached to the Condensable Propellant Facility, shown in Figure 10. Design and construction work was initiated prior to testing of the XOCOT-T. Depending on the outcome of the design investigation some of the aspects of the original design may change.

The discharge circuit will not be optimized in this research, since high power switching hardware has already been purchased. The switches to be used are mercury filled ignitrons which can operate under

high power loads but add a significant amount of inductance ($1.5 \mu\text{H}$) to the system. While this will tremendously increase the overall inefficiency of the system, it can be accounted for by only considering the voltage drop across the coils.

Diagnostics planned for the TeXOCOT experiment include current and voltage monitors, diamagnetic flux loops, internal and external magnetic field probes, internal triple probes, and a ballistic pendulum. Current and voltage monitors will be used to measure the current passing through each coil, the charging voltage on the capacitor bank, and the voltage drop across the coils. Diamagnetic flux loops and external magnetic field probes will measure the magnetic field from AFRC formation activities inside the discharge coils, to indicate the presence of an AFRC. Three axis magnetic field probes, spatially separated can also track the plasmoid as it leaves the coils.

A time-of-flight array consisting of triple probes (30) and magnetic field probes (31) can provide average velocity measurements of the traveling plasmoid. The triple probes, placed a set axial distance from each other downstream of the formation chamber, will record a time history of plasma traveling past them. The waveforms registered by each probe will be compared to magnetic field probe data, recorded by probes placed very close to the triple probes, to determine if and which portion of the plasma has a magnetic field structure (which would indicate an AFRC). The time it takes for the AFRC to travel from one probe to the next, knowing the separation between the probes, will give an estimate for the average velocity of the plasmoid.

A ballistic pendulum (32) located downstream can measure the plasmoid's kinetic energy (and momentum) so that its mass can be estimated. A ballistic pendulum relies on the impact of the plasmoid against the swinging arm of the pendulum. Upon collision, the plasmoid "sticks" to the pendulum, transfers its kinetic energy to the pendulum, causes it to swing upwards, resulting in a change in potential energy of the pendulum-plasmoid system. If the impact velocity v of the plasmoid is known (can be inferred from time-of-flight measurements), the mass of the plasmoid m_{plasmoid} can be found using the conservation of energy relation combined with conservation of momentum, giving:

$$m_{\text{plasmoid}} = \frac{m_{\text{pendulum}} \sqrt{2gh}}{v_1 - \sqrt{2gh}} \quad (14)$$

where m_{pendulum} is the mass of the pendulum, v_1 is the velocity of the plasmoid, g is the acceleration from gravity, and h is maximum height of the pendulum after impact. As part of this research, a pendulum will need to be designed to capture all of the plasmoid mass, with minimal erosion of the pendulum from high energy ions. The mechanism that measures the height of the pendulum arm will need to have a rapid response time and low noise pick-up.

Efficiency analysis can be accomplished by comparing the plasmoid's final velocity (measured with the time-of-flight array) and mass (from ballistic pendulum) to the energy in the capacitor (minus switching losses). These values can be inserted into equation 13 to estimate the overall system efficiency. Though this method depends on measurements from a time-of-flight array, and a ballistic pendulum, all which have a considerable errors (20 percent) associated with them, it should provide a qualitative measure of the efficiency expected from a system.

7 Time Line and Management Plan

The research proposed in this document is expected to take 20 months to complete, with a tentative completion date slated for December 2010. The final presentation of this research is expected to occur in mid-April



Figure 10: The AFRC experiment under construction in MTU's ISP Lab.

Table 4: Research Timeline			
Task	Expected Duration	Start Date	End Date
Scaling Analysis			
and Launcher Model Refinement	1 month	5-1-2009	5-31-2009
Magnetic Field Modeling (XOCOT-T)	1 month	6-1-2009	6-30-2009
Parameter Investigation			
and Experimental Design	1 month	7-1-2009	7-31-2009
Discharge Circuit Construction	1 month	8-1-2009	8-31-2009
Stationary Plasma Experiments	3 months	9-1-2009	11-30-2009
Translation Experiment Construction			
and Initial Testing	2 months	12-1-2009	1-31-2010
Translation Studies	11 months	2-1-2010	12-31-2010
Dissertation Preparation	4 months	1-1-2011	4-15-2011

2011. An outline has been made of important tasks, time allotted, anticipated start and completion dates. This schedule is outlined in Table 4.

Translation studies are expected to consume the largest block of time, starting in February 2010 and ending December 2010. This will allow ample time for a in-depth study of the available operating conditions for the TeXOCOT. To ensure important completion dates are met, monthly reports will be completed and reviewed by select committee members. Conference papers and journal articles will not only document the project, but provide further incentive for task completion.

The schedule provides a great deal of flexibility which is required in experimental endeavors, making accommodations for equipment failures, on-the-go design modifications, and experimental mishaps. As the author has learned from previous high pulsed power experimentation work, high power pulsed systems do not fail conveniently, cheaply, or quietly. Plenty of time must be left for frequent reassembly and disassembly, back-ordered replacement hardware, and ground loop troubleshooting.

8 Summary: Significance of Proposed Work

Annular field reversed configurations (AFRC) plasma devices may provide an innovative solution to efficient high power electric propulsion at attainable power levels. Though formation of AFRCs has been demonstrated in multiple experiments, successful translation studies on AFRCs have never been published. This research proposes to fill this void by investigating AFRC translation using numerical studies and experimental methods. These studies will help determine if AFRCs are a viable high power electric propulsion technology.

The numerical tools developed for this research will be used to see how the AFRC compares to similar technologies such as the spheromak thruster and the PIT. Comparing this device against similar devices improves collaboration among the propulsion community by promoting discussions, sharing technological advances, and merging ideas.

This research has the potential to reach beyond the space propulsion community; AFRCs developed originally as an low-voltage approach to fusion. Providing information on their translation dynamics may provide incentive for further development for fusion. This research can encourage the collaboration of several fields of research with its cross-discipline aspects, common in experimental plasma studies. Frequent consultation with members of the electrical engineering, physics, and mechanical engineering departments can provide new insight into old ideas. The University setting is ideal not only for this type of collaboration, but for introducing undergraduates to the realm of scientific research. Allowing them a chance to get involved in research may open doors and enable opportunities that are not readily apparent in a traditional curriculum. It will also give the future generation of research scientists and engineers an opportunity to teach advanced concepts at a fundamental level and to interact outside of their peer group. The benefits this research has on society push beyond technological solutions to promote education, cooperation, and scientific discovery.

References

- [1] Pietrzyk, Z., Vlasses, G., Brooks, R., Hahn, K., and Raman, R., "Initial Results from the Coaxial Slow Source FRC Device," *Nuclear Fusion*, Vol. 27, No. 9, 1987, pp. 1478–89.
- [2] Phillips, J., "Proposal to Produce Large Compact Toroids," Report LA-8711-P, Los Alamos National Laboratory, March 1981.
- [3] Berger, R., *Analysis of Slow Formation of Plasmas in a Coaxial Double Theta Pinch*, Phd thesis, University of Washington, 1993.
- [4] Kirtley, D. E., *Study of the Synchronous Operation of an Annular Field Reversed Configuration Device*, Phd thesis, University of Michigan, Ann Arbor, MI, 2008.
- [5] Pierce, W., Maqueda, R., Brooks, R., and Farengo, R., "Initial Results from Parallel Coil Operation of the Coaxial Slow Source Field Reversed Configuration Device," *Nuclear Fusion*, Vol. 33, 1993, pp. 117–132.
- [6] Tuszewski, M., "Field Reversed Configurations," *Nuclear Fusion*, Vol. 28, 1988, pp. 2033–2092.
- [7] Rej, D. J., Armstrong, W. T., Chrien, R. E., Klingner, P. L., Linford, R. K., McKenna, K. F., Sherwood, E. G., Simeon, R. E., Tuszewski, M., and Milroy, R. D., "Experimental studies of field-reversed configuration translation," *Physics of Fluids*, Vol. 29, No. 3, Mar 1986, pp. 852–862.
- [8] Tanjyo, M., Okada, S., Ito, Y., Kako, M., Ohi, S., Goto, S., Ishimura, T., and Ito, H., "Translation Experiment of a Plasma with Field Reversed Configuration," *Technology Reports of the Osaka University*, Vol. 34, No. 1763, Oct 1984, pp. 201–210.
- [9] Greve, P., Haumann, J., Kunze, H. J., and Ullrich, L. K., "Effects of an Inhomogeneous Impurity Distribution in a Field-Reversed Theta-Pinch," *Physics of Fluids*, Vol. 25, No. 3, 1982, pp. 452–456.
- [10] Alidieres, M., Aymar, R., Jourdan, P., and Koechlin, F., "Experimental Study of a Current Sheet," *Plasma Physics*, Vol. 10, 1968, pp. 841–850.
- [11] Kondoh, Y., Nagao, S., Futawatari, N., and Itoh, K., "An experiment of Double Theta-Pinch," *Japanese Journal of Applied Physics*, Vol. 13, No. 6, 1974, pp. 1037–1038.
- [12] Niemela, C. S. and Kirtley, D. E., "Initial Results on an Annular Field Reversed Configuration Plasma Translation Experiment," *Proceedings of the 6th MS/4th LPS/3rd SPS Joint Subcommittee Meeting*, No. TP-2008-489, JANNAF, Orlando, FL, December 2008, Distribution A.
- [13] Tuszewski, M., Armstrong, W. T., Chrien, R. E., Klingner, P. L., McKenna, K. F., Rej, D. J., Sherwood, E. G., and Simeon, R. E., "Confinement of translated field-reversed configurations," *Physics of Fluids*, Vol. 29, No. 3, Mar 1986, pp. 863–870.
- [14] Intrator, T. P., Siemon, R. E., and Sieck, P. E., "Adiabatic model and design of a translating field reversed configuration," *Physics of Plasmas*, Vol. 15, No. 4, 2008, pp. 042505–10.
- [15] Guo, H. Y., Hoffman, A. L., Brooks, R. D., Peter, A. M., Pietrzyk, Z. A., Tobin, S. J., and Votroubek, G. R., "Formation and steady-state maintenance of field reversed configuration using rotating magnetic field current drive," *Physics of Plasmas*, Vol. 9, No. 1, 2002, pp. 185–200.
- [16] Slough, J. T., Blair, A., Pihl, C., and Votroubek, G., "Magnetically Accelerated Plasmoid (MAP) Thruster - Initial Results and Future Plans," *30th International Electric Propulsion Conference*, No. IEPC-2007-16.
- [17] Jahn, R. G., *Physics of Electric Propulsion*, Dover Publications, Mineola, NY, 1968.
- [18] Dailey, C. L. and Lovberg, R., "The PIT MkV Pulsed Inductive Thruster," NASA Contractor Report 191155, July 1993.
- [19] Choueiri, E. Y. and Polzin, K. A., "Faraday acceleration with radio-frequency assisted discharge," *Journal of Propulsion and Power*, Vol. 22, No. 3, 2006, pp. 611–619.

- [20] Hallock, A. K., Choueiri, E. Y., and Polzin, K. A., "Current Sheet Formation in a Conical Theta Pinch Faraday Accelerator with Radio-frequency Assisted Discharge," *30th International Electric Propulsion Conference*, No. IEPC-2007-165.
- [21] Koelfgen, S., Hawk, C., Eskridge, R., Lee, M., Martin, A., and Smith, J., "A Plasmoid Thruster for Space Propulsion," *Proceedings of the 39th Joint Propulsion Conference and Exhibit*, No. AIAA-2003-4992, Huntsville, AL, July 2003.
- [22] Eskridge, R. and Martin, A., "Progress on the PT-1 Prototype Plasmoid Thruster," Tech. Rep. 200800006053, NASA Marshall Space Flight Center, October 17-19 2007.
- [23] Martin, A. and Eskridge, R., "Electrical coupling efficiency of inductive plasma accelerators," *Journal of Physics D-Applied Physics*, Vol. 38, No. 23, 2005, pp. 4168–4179.
- [24] Polzin, K. A. and Choueiri, E. Y., "Performance optimization criteria for pulsed inductive plasma acceleration," *IEEE Transactions on Plasma Science*, Vol. 34, No. 3, 2006, pp. 945–953.
- [25] Novac, B. M., Smith, I. R., Enache, M. C., and Senior, P., "Studies of a very high efficiency electromagnetic launcher," *Journal of Physics D-Applied Physics*, Vol. 35, No. 12, 2002, pp. PII S0022–3727(02)33567–8.
- [26] Spitzer, L. J., *Physics of Fully Ionized Gases*, Vol. 3 of *Interscience Tracts on Physics and Astronomy*, Interscience Publishers, Inc., New York, 1956.
- [27] Grover, F. W., *Inductance Calculations: Working Formulas and Tables*, Dover Publications, Inc., New York, NY, 2nd ed., 1973.
- [28] Lundin, R., "A handbook formula for the inductance of a single-layer circular coil," *Proceedings of the IEEE*, Vol. 73, No. 9, 1985, pp. 1428–1429.
- [29] Cassibry, J. T., "Comparison of Directly and Inductively Coupled Pulsed Electromagnetic Thrusters," *IEEE Transactions on Plasma Science*, Vol. 36, No. 5, 2008, pp. 2180–2188.
- [30] Chang, J.-S., Ogram, G., Hobson, R., and Teii, S., "The instantaneous triple-probe method for the direct display of plasma parameters in a low density continuum plasma," *Journal of Physics D: Applied Physics*, Vol. 13, 1980, pp. 1083–1092.
- [31] Phillips, R. and Turner, E., "Construction and Calibration Techniques of High Frequency Magnetic Probes," *The Review of Scientific Instruments*, Vol. 36, No. 12, 1965, pp. 1822–1825.
- [32] Yoshinori, T., Koji, E., and Kouichi, O., "A miniature electrothermal thruster using microwave-excited microplasmas: Thrust measurement and its comparison with numerical analysis," *Journal of Applied Physics*, Vol. 101, No. 12, 2007, pp. 123307.